JOURNAL OF AIRCRAFT
Vol. 35, No. 4, July–August 1998

Sensitivity Analysis for Transonic Unsteady Aeroelastic Constraints

R. M. Kolonay* and V. B. Venkayya†
U.S. Air Force Research Laboratory, Wright–Patterson Air Force Base, Ohio 45433
and
Henry T. Y. Yang‡
University of California, Santa Barbara, Santa Barbara, California 93106

A method for calculating the sensitivities for transonic unsteady aeroelastic constraints with respect to structural design variables consisting of skin thicknesses, spar thicknesses, spar cap cross-sectional areas, and concentrated masses for flight vehicles in three-dimensional fluid flow is presented. The method requires that the transonic unsteady aerodynamics be represented in the frequency or Laplace domain. In this work the indicial response method is used to transform time-domain aerodynamics found by solving the transonic small disturbance (TSD) equations into the Laplace domain. The indicial responses are performed about a static aeroelastic equilibrium found using the TSD equations for the steady aerodynamics. Once in the Laplace domain, the unsteady aerodynamics are used to develop semianalytic equations for the constraint sensitivities. These sensitivity equations include a nonlinear term that is calculated by finite differences at a considerable computational cost. This term arises because the indicial responses are performed about a static aeroelastic equilibrium. If a static rigid equilibrium is used instead, this term vanishes, producing fully analytic sensitivities. In addition, for the test cases chosen, it is found that this nonlinear term contributed little to the total gradient calculation and could be ignored. This method of sensitivity calculation enables formal unsteady aeroelastic optimization in the transonic flight regime.

Nomenclature

$[B]$ = damping matrix
$[\bar{B}]$ = generalized damping, $[\Phi]^T[B][\Phi]$
b = reference semichord
$b_{r_{ij}}$ = coefficient in Laplace representation of unsteady aerodynamics
C_p^L, C_p^U = lower surface pressure coefficient, upper surface pressure coefficient
C_R = reference chord
$C_{r_{ij}}$ = coefficient in Laplace representation of unsteady aerodynamics
GFACT = constraint normalization factor
$\mathcal{J}(p)$ = imaginary part of p
i $\equiv \sqrt{-1}$
$[K]$ = structural stiffness
$[\bar{K}]$ = generalized stiffness, $[\Phi]^T[K][\Phi]$
k = reduced frequency, based on semichord
$[M]$ = structural mass
$[\bar{M}]$ = generalized mass, $[\Phi]^T[M][\Phi]$
M_∞ = freestream Mach number
m = number of structural modes participating in the analysis/design
p $\equiv k(\gamma + i)$, complex response frequency/eigenvalue
$[Q(p)]$ = generalized aerodynamic matrix
q_f = flutter dynamic pressure
$\{\boldsymbol{q}(\boldsymbol{p})\}$ = eigenvector of modal coordinates
$\mathcal{R}(p)$ = real part of p
U_f = flutter velocity
U_∞ = freestream airspeed
$\boldsymbol{v}_s$ = vector of design variables
$\{\boldsymbol{y}\}^T$ = left-hand eigenvector of flutter equation
Z_j = normalized constraint
α_0 = static initial angle of attack
γ = damping factor
ΔC_P = $C_p^L - C_p^U$
ρ_∞ = freestream air density
$[\Phi]$ = set of orthogonal structural eigenvectors
ω_f = flutter frequency
ω_l = structural natural frequency

Received Oct. 5, 1996, revision received Sept. 10, 1997; accepted for publication Oct. 10, 1997.

*Aerospace Engineer, Structures Division, Flight Dynamics Directorate; currently at General Electric Corporate R&D Center, Building K-1, Room 2A60, 1 Research Center, Niskayuna, NY 12309. Member AIAA.

†Research Aerospace Engineer, Structures Division, Flight Dynamics Directorate. Fellow AIAA.

‡Professor and Chancellor, Department of Mechanical and Environmental Engineering. Fellow AIAA.

Introduction

MULTIDISCIPLINARY optimization of aircraft structures requires engineering analyses throughout the flight regime. Well-established techniques exist for incorporating unsteady subsonic/supersonic aeroelastic (flutter) analysis/constraints in the multidisciplinary design environment.[1,2] To date, minimal work specifically associated with structural design subject to transonic flutter constraints has been presented in the open literature. The most recent and closely related works to the research reported here are the investigations done by Kapania et al.[3,4] They calculated analytically and by finite differences the sensitivities of flutter speed with respect to structural parameters using transonic aerodynamics for a two-dimensional airfoil. The unsteady aerodynamics Kapania et al.[3,4] used were the analytic indicial response functions developed by Leishman and Nguyen.[5] The structural parameters considered were those found in the two-degree-of-freedom aeroelastic equations of motion: mass ratio, static unbalance, radius of gyration, bending frequency, and torsional frequency. Another related area where much effort has been placed recently is in the calculation of sensitivities of aerodynamic configuration parameters in the presence of nonlinear aerodynamics. This consists of determining the sensitivities of aerodynamic param-

eters, e.g., thickness-to-chord ratio, airfoil shape, and planform, with respect to aerodynamic performances such as lift and drag using nonlinear aerodynamics. As stated by Korivi et al.,[6] these types of sensitivities can be calculated in three ways; 1) finite differences, 2) the discrete approach (differentiation of governing equations following their discretization), and 3) the continuum approach (differentiation of governing equations prior to numerical discretization). Korivi et al.[6] cited many efforts using the discrete approach applied to all levels of computational fluid dynamics (CFD), and the work performed by Jorggaard and Burns[7] demonstrated the continuum approach.

The difficulties associated with transonic flutter analysis is because of the introduction of nonlinearities into the problem through the transonic aerodynamic fluid flow. Transonic flow is characterized by mixed subsonic and supersonic flow with shocks. To accurately predict the aerodynamic pressures in the transonic region, nonlinear partial differential equations must be solved. This paper presents the development of a sensitivity analysis for flutter constraints in the transonic regime suitable for the multidisciplinary preliminary design environment.

In this study it is assumed that, at a given static aeroelastic equilibrium position, the change in dynamic angle of attack about that equilibrium is small. This assumption implies that the aerodynamic forces and shock movement will be linear with a change in the dynamic angle of attack. These assumptions enable time-domain computational fluid aerodynamics to be curve fit into the Laplace domain.[8,9] This permits the writing of linear unsteady aeroelastic equations of motion. Once the aeroelastic equations of motion are written, techniques such as the p method or the pk method can be used to determine the unsteady aeroelastic response.[9] This paper uses the linear unsteady aeroelastic equations and develops semianalytic equations for the sensitivity analysis of the structural design variables with respect to the unsteady aeroelastic constraints. Once the constraint values and gradients are determined, a nonlinear mathematical programming problem can be formulated for design. For this work the finite element method is used to represent the mass/stiffness distribution of the structure, and the transonic small disturbance (TSD) equations are used to model the steady and unsteady aerodynamics.

Flutter Constraint

Using the p method for the flutter analysis the fundamental equation of motion can be written as[10]

$$\left[\left(\frac{U_\infty}{b}\right)^2 p^2[\bar{M}] + \left(\frac{U_\infty}{b}\right) p[\bar{B}] + [\bar{K}] - \frac{1}{2}\rho_\infty U_\infty^2[\bar{Q}(p)]\right] \times \{\boldsymbol{q}(\boldsymbol{p})\} = 0 \tag{1}$$

The flutter constraint is defined by satisfying requirements on modal damping at a series of velocities rather than on the actual flutter speed.[2,10,11] This can be expressed as

$$\gamma_{lj} \leq \gamma_{j\text{REQ}} \quad \begin{matrix} j = 1, 2 \ldots \text{number of velocities} \\ l = 1, 2 \ldots \text{number of modes} \end{matrix} \tag{2a}$$

or

$$Z_j = \frac{\gamma_{lj} - \gamma_{j\text{REQ}}}{\text{GFACT}} \leq 0 \tag{2b}$$

Where $\gamma_{j\text{REQ}}$ is the required level of damping at the jth velocity, and γ_{lj} is the calculated damping value for the lth mode at the jth velocity. GFACT is used to scale the constraint value. GFACT must be used because normalization cannot be done by $\gamma_{j\text{REQ}}$ in view of the fact that $\gamma_{j\text{REQ}}$ can take on the value of zero. For this research a value of 0.1 for GFACT is used in all cases studied.

Sensitivity of Flutter Constraint with Respect to Structural Design Variables

Let $\boldsymbol{v}_s$ be defined as a vector of design variables that are directly related to the properties of finite elements such as thicknesses, cross-sectional areas, and concentrated mass values. The derivative of the constraint in Eq. (2) with respect to the design variable is

$$\frac{\partial Z_j}{\partial \boldsymbol{v}_s} = \frac{1}{\text{GFACT}} \frac{\partial \gamma_{lj}}{\partial \boldsymbol{v}_s} \tag{3}$$

Using the definition of p in Eq. (1) results in the following representation of γ (the subscripts on γ will be dropped from now on):

$$\gamma = (p/k) - i \tag{4}$$

Differentiating Eq. (4) with respect to $\boldsymbol{v}_s$ and realizing that γ is real and, therefore, so is $\partial\gamma/\partial\boldsymbol{v}_s$, yields

$$\frac{\partial \gamma}{\partial \boldsymbol{v}_s} = \frac{1}{k}\left[\frac{\partial}{\partial \boldsymbol{v}_s}\Re(p) - \gamma \frac{\partial}{\partial \boldsymbol{v}_s}\Im(p)\right] \tag{5}$$

The gradient of the eigenvalue p can be found by differentiating Eq. (1). Restating Eq. (1) in the following form:

$$[\Phi]^T[W][\Phi]\{\boldsymbol{q}\} = 0 \tag{6}$$

with the adjoint relation

$$\{\boldsymbol{y}\}^T[\Phi]^T[W][\Phi] = 0 \tag{7}$$

where $[W]$ contains the system matrices in physical coordinates. Differentiating Eq. (6) with respect to $\boldsymbol{v}_s$ and premultiplying by $\{\boldsymbol{y}\}^T$ gives

$$\{\boldsymbol{y}\}^T \frac{\partial}{\partial \boldsymbol{v}_s}[\Phi]^T[W][\Phi]\{\boldsymbol{q}\} + \{\boldsymbol{y}\}^T[\Phi]^T \frac{\partial}{\partial \boldsymbol{v}_s}[W][\Phi]\{\boldsymbol{q}\} + \{\boldsymbol{y}\}^T[\Phi]^T[W]\frac{\partial}{\partial \boldsymbol{v}_s}[\Phi]\{\boldsymbol{q}\} + \{\boldsymbol{y}\}^T[\Phi]^T[W][\Phi]\frac{\partial}{\partial \boldsymbol{v}_s}\{\boldsymbol{q}\} = 0 \tag{8}$$

Using Eq. (7), which indicates that the last term in Eq. (8) vanishes, yields

$$\{\boldsymbol{y}\}^T \frac{\partial}{\partial \boldsymbol{v}_s}[\Phi]^T[W][\Phi]\{\boldsymbol{q}\} + \{\boldsymbol{y}\}^T[\Phi]^T \frac{\partial}{\partial \boldsymbol{v}_s}[W][\Phi]\{\boldsymbol{q}\} + \{\boldsymbol{y}_h\}^T[\Phi]^T[W]\frac{\partial}{\partial \boldsymbol{v}_s}[\Phi]\{\boldsymbol{q}\} = 0 \tag{9}$$

Following the procedure developed by Rudisill and Bhatia[12] and further refined by Haftka and Yates,[13] the structural modes are assumed to be a basis for the system. With this assumption $[\Phi]$ is considered invariant with respect to $\boldsymbol{v}_s$ and, thus, the $\partial[\Phi]^T/\partial\boldsymbol{v}_s$, $\partial[\Phi]/\partial\boldsymbol{v}_s$ terms in Eq. (9) are assumed zero. This assumption is valid for small increments in the design variables. The more modes retained for representing the basis of the system, the larger the increment allowed in the design variables. Reference 10 makes a similar assumption and Refs. 13 and 14 give discussions of the effects of this assumption. With this in mind, Eq. (9) can be expanded and takes the form

$$\{\boldsymbol{y}\}^T\left[2p\left(\frac{U_\infty}{b}\right)^2\frac{\partial p}{\partial \boldsymbol{v}_s}[\bar{M}] + \left(\frac{U_\infty}{b}\right)^2 p^2\frac{\partial}{\partial \boldsymbol{v}_s}[\bar{M}] + \left(\frac{U_\infty}{b}\right)\frac{\partial p}{\partial \boldsymbol{v}_s}[\bar{B}] + p\left(\frac{U_\infty}{b}\right)\frac{\partial}{\partial \boldsymbol{v}_s}[\bar{B}] + \frac{\partial}{\partial \boldsymbol{v}_s}[\bar{K}] - \frac{1}{2}\rho_\infty U_\infty^2\frac{\partial}{\partial \boldsymbol{v}_s}[\bar{Q}(p)]\right]\{\boldsymbol{q}\} = 0 \tag{10}$$

Equation (10) involves the derivatives of the generalized mass, stiffness, damping, and aerodynamic matrices with respect to the design variables. Reference 10 shows the calculation of these terms along with the determination of $\partial\gamma/\partial v_s$ for unsteady aerodynamics calculated by the doublet lattice method. For the doublet lattice method the $[Q(p)]$ matrix is dependent on M_∞ and k. This allows for straightforward calculation of the $\partial[\bar{Q}(p)]/\partial v_s$ term in Eq. (10). For the linearized TSD, unsteady aerodynamics $[\bar{Q}(p)]$ is not only a function of M_∞ and k (p in this case), but also a function of the initial conditions and the static aeroelastic equilibrium position. Also note that $[\bar{Q}(p)]$ is a function of the eigenmatrix $[\Phi]$, but recalling the previous assumption concerning $\partial[\Phi]/\partial v_s$ implies that the sensitivities of these terms are zero for small increments in the design variables. Using the approximation for $[\bar{Q}(p)]$ developed in Refs. 8 and 9, $[\bar{Q}(p)]$ can be expressed in terms of p as

$$[\bar{Q}(p)] = \bar{Q}_{ij}(p) = 4b^2 \sum_{r=1}^{n} 2p \left(\frac{C_{r_{ij}}}{2p + b_{r_{ij}}}\right) \tag{11}$$

Where $C_{r_{ij}}$ and $b_{r_{ij}}$ are determined by curve fitting the time-domain indicial responses, and the ij subscripts represent the ijth entry in the $[\bar{Q}(p)]$ matrix. Because $[\bar{Q}(p)]$ is found through a set of equations that were developed in modal coordinates, i.e., it depends on the natural frequencies of the structure ω_l, the chain rule of differentiation can be applied to Eq. (11) to determine the derivative of the generalized aerodynamic matrix with respect to the design variables. This yields

$$\frac{\partial}{\partial v_s}[\bar{Q}(p)] = 4b^2 \left[\frac{\partial}{\partial p}[\bar{Q}(p)]\left(\frac{\partial p}{\partial v_s}\right) + \sum_{l=1}^{m}\left(\frac{\partial}{\partial \omega_l}[\bar{Q}(p)]\right)\left(\frac{\partial \omega_l}{\partial v_s}\right)\right] \tag{12}$$

Substituting this into Eq. (10) gives

$$\{y\}^T\left[2p\left(\frac{U_\infty}{b}\right)^2\frac{\partial p}{\partial v_s}[\bar{M}] + \left(\frac{U_\infty}{b}\right)^2 p^2\frac{\partial}{\partial v_s}[\bar{M}] + \left(\frac{U_\infty}{b}\right)\frac{\partial p}{\partial v_s}[\bar{B}] + p\left(\frac{U_\infty}{b}\right)\frac{\partial}{\partial v_s}[\bar{B}] + \frac{\partial}{\partial v_s}[\bar{K}] - \frac{1}{2}\rho_\infty U_\infty^2(4b^2)\left[\frac{\partial}{\partial p}[\bar{Q}(p)]\left(\frac{\partial p}{\partial v_s}\right) + \sum_{l=1}^{m}\left(\frac{\partial}{\partial \omega_l}\bar{Q}[(p)]\right)\left(\frac{\partial \omega_l}{\partial v_s}\right)\right]\right]\{q\} = 0 \tag{13}$$

Noting that every term in Eq. (13) is a complex scalar, $\partial p/\partial v_s$ can be found to be

$$\frac{\partial p}{\partial v_s} = \left[-p^2\left(\frac{U_\infty}{b}\right)^2\{y\}^T\frac{\partial}{\partial v_s}[\bar{M}]\{q\} - p\left(\frac{U_\infty}{b}\right)\{y\}^T\frac{\partial}{\partial v_s}[\bar{B}]\{q\} - \{y\}^T\frac{\partial}{\partial v_s}[\bar{K}]\{q\} + \frac{1}{2}\rho_\infty U_\infty^2(4b^2)\{y\}^T\left[\sum_{l=1}^{m}\left(\frac{\partial}{\partial \omega_l}\bar{Q}[(p)]\right)\left(\frac{\partial \omega_l}{\partial v_s}\right)\right]\{q\}\right] \Bigg/ \left[2p\left(\frac{U_\infty}{b}\right)^2\{y\}^T[\bar{M}]\{q\} + \left(\frac{U_\infty}{b}\right)\{y\}^T[\bar{B}]\{q\} - \frac{1}{2}\rho_\infty U_\infty^2(4b^2)\{y\}^T\frac{\partial}{\partial p}[\bar{Q}(p)]\{q\}\right] \tag{14}$$

Here $\partial p/\partial v_s$ is, in general, a complex quantity that can be used to complete the evaluation of $\partial\lambda/\partial v_s$ in Eq. (5). All terms in Eq. (14) can be found analytically except for the term $\partial[\bar{Q}(p)]/\partial\omega_l$, which must be determined numerically. The derivative of terms containing the mass, stiffness, damping, and natural frequencies with respect to the design variable are determined using the procedures in Ref. 10. They are excluded here for briefness.

The two remaining terms needed to complete the evaluation of Eq. (14) are $(\partial/\partial p)[\bar{Q}(p)]$ and $\partial[\bar{Q}(p)]/\partial\omega_l$. The first term $(\partial/\partial p)[\bar{Q}(p)]$ can be found explicitly by differentiating Eq. (11) with respect to p, with $4b^2$ factored out earlier

$$\frac{\partial}{\partial p}[\bar{Q}(p)] = 2\sum_{r=1}^{n}\frac{C_{r_{ij}}}{2p + b_{r_{ij}}} - \sum_{r=1}^{n}\frac{4pC_{r_{ij}}}{(2p + b_{r_{ij}})^2} \tag{15}$$

The second term $\partial[\bar{Q}(p)]/\partial\omega_l$ is not so easily computed. This term must be found numerically. For this work the term is computed by forward finite difference.

It is worthwhile to discuss the computational cost of evaluating Eq. (14). When using the indicial response method, if m structural modes are kept in the analysis then $m + 1$ (one

Table 1 Rectangular wing modes

Mode	Frequency, Hz	Mode type
1	1.9789	First bending
2	3.9224	First torsion

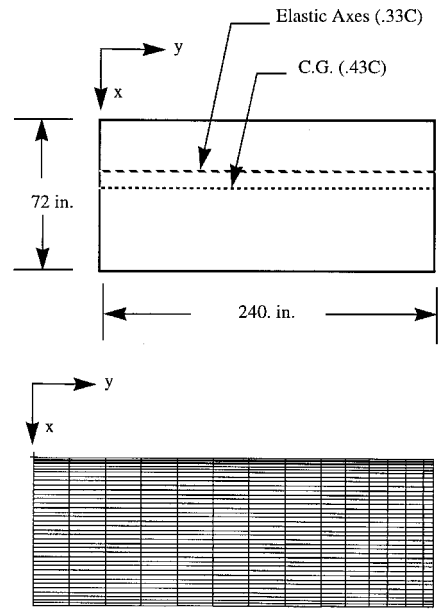

Fig. 1 Rectangular wing planform and CFD mesh (39 × 15 on wing).

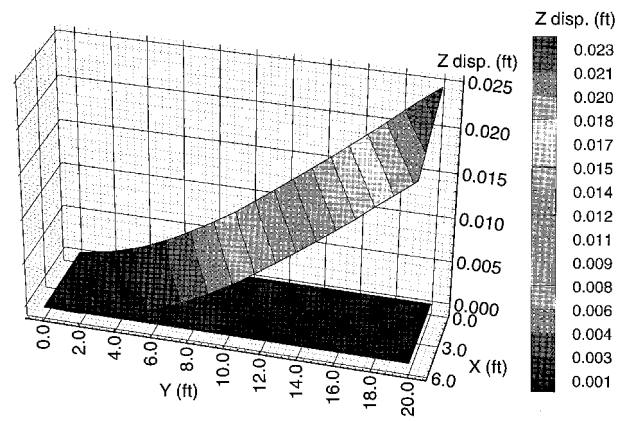

Fig. 2 Rectangular wing static aeroelastic deformation (M_∞ = 0.85, α_0 = 0.5 deg, and q_∞ = 86.0 psf).

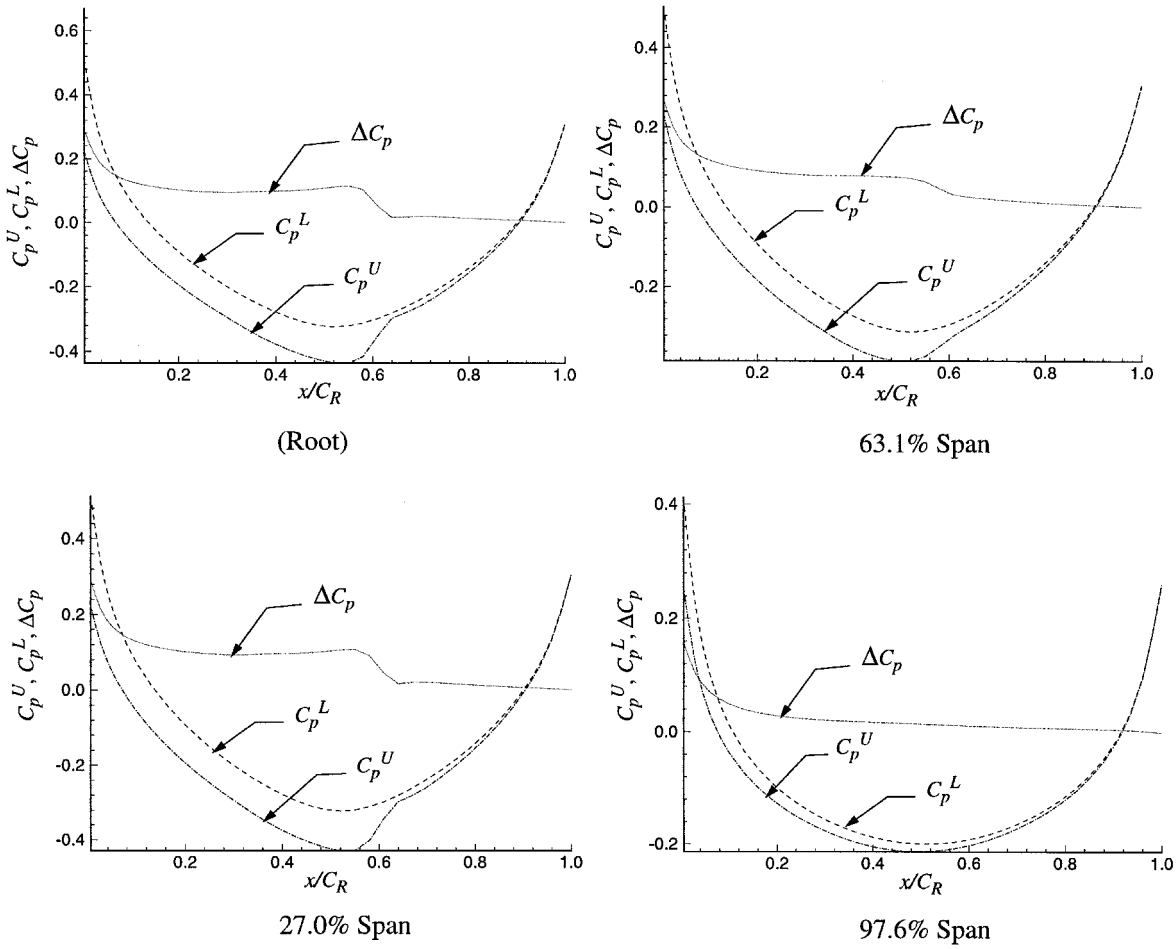

Fig. 3 Rectangular wing aeroelastic pressure coefficients ($M_\infty = 0.85$, $\alpha_0 = 0.5$ deg, and $q_\infty = 86.0$ psf).

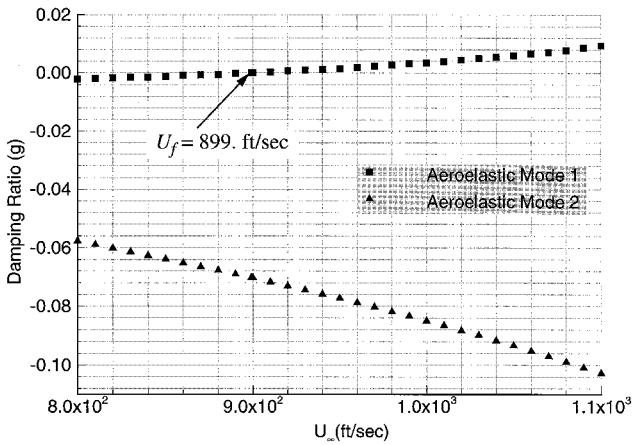

Fig. 4 Rectangular wing U_∞ vs g ($M_\infty = 0.85$, $\alpha = 0.5$ deg, and $\rho_\infty = 1.910\text{E}{-}04$ slugs/ft^3).

for the static aeroelastic solution and m for the indicial responses) CFD time integrations are required to get the unsteady aerodynamics in the Laplace domain. Because all of Eq. (14) is analytic except for $\partial[Q(p)]/\partial\omega_I$, no additional CFD solutions would be required if the $\partial[\bar{Q}(p)]/\partial\omega_I$ term could be ignored. To calculate the $\partial[\bar{Q}(p)]/\partial\omega_I$ term by forward finite differences requires an additional $m(m + 1)$ time integration. This $m(m + 1)$ results from m time integrations for the perturbation of each ω_I to calculate the perturbed static aeroelastic equilibrium, and $m \times m$ time integrations to perform the indicial responses about these perturbed static aeroelastic states. It is also important to note that if the static equilibrium is a rigid solution instead of an aeroelastic solution, the $\partial[\bar{Q}(p)]/\partial\omega_I$ is identically zero. Therefore, it is essential to evaluate the contribution of $\partial[\bar{Q}(p)]/\partial\omega_I$ to the total gradient and determine if it can be neglected, thus resulting in significant savings of computational effort. Finally, if the $\partial[\bar{Q}(p)]/\partial\omega_I$ could be found by differentiating the static aeroelastic equations, the number of additional time integrations to determine the sensitivities would be reduced to m.

Table 2 Rectangular wing constraint value[a]

Mode number	Constraint value @, ft/s			
	800	850	1000	1150
1	−0.01035	−0.00576	0.01742	0.06940
2	−0.28870	−0.31910	−0.42490	−0.56820

[a] $M_\infty = 0.85$, $\alpha = 0.5$ deg, and $\rho_\infty = 1.910\text{E}{-}04$ slugs/ft^3.

Sensitivity Analysis Examples

To demonstrate the preceding derivations two wing models are considered. The first is a rectangular, unswept, untapered planform that uses a beam representation for the structure. The second is a swept, tapered, fighter planform where the structure is represented by a built-up finite element wing box. A Cray Y-MP is employed for all of the TSD computations, therefore some computer resource usage is reported on these examples. The intent of presenting the computer resource information is to give a rough order-of-magnitude estimate on the time necessary to perform the calculations, and as a basis of comparison for the different computations done within the present research.

Table 3 Rectangular wing gradient terms[a]

$\frac{\partial Z_j}{\partial v_s}$	Includes $\frac{\partial[\bar{Q}]}{\partial v_s}$, no $\frac{\partial[\bar{Q}]}{\partial[\Phi]}$, $\frac{\partial[\Phi]}{\partial v_s}$		No $\frac{\partial[\bar{Q}]}{\partial v_s}$, no $\frac{\partial[\bar{Q}]}{\partial[\Phi]}$, $\frac{\partial[\Phi]}{\partial v_s}$		Includes $\frac{\partial[\bar{Q}]}{\partial v_s}$, includes $\frac{\partial[\bar{Q}]}{\partial[\Phi]}$, $\frac{\partial[\Phi]}{\partial v_s}$
	Analytical	Finite difference	Analytical	Finite difference	Finite difference
$\frac{\partial Z_{U_\infty}}{\partial v_1} = 800$	−0.5442	−0.5453	−0.5653	−0.5648	−0.5423
$\frac{\partial Z_{U_\infty}}{\partial v_1} = 850$	−0.7262	−0.7267	−0.7455	−0.7445	−0.7220
$\frac{\partial Z_{U_\infty}}{\partial v_1} = 1000$	−1.7099	−1.7091	−1.7345	−1.7332	−1.7104
$\frac{\partial Z_{U_\infty}}{\partial v_1} = 1150$	−4.4704	−4.4656	−4.5144	−4.5110	−4.4948
$\frac{\partial Z_{U_\infty}}{\partial v_2} = 800$	0.0156	0.0149	0.0191	0.0188	0.0166
$\frac{\partial Z_{U_\infty}}{\partial v_2} = 850$	0.0136	0.0130	0.0183	0.0183	0.0146
$\frac{\partial Z_{U_\infty}}{\partial v_2} = 1000$	0.0000	−0.0011	0.0069	0.0069	0.0027
$\frac{\partial Z_{U_\infty}}{\partial v_2} = 1150$	−0.0532	−0.0549	−0.0456	−0.0465	−0.0431

[a] $M_\infty = 0.85$, $\alpha_0 = 0.5$ deg, and $\rho_\infty = 1.910\text{E}{-}04$ slugs/ft^3.

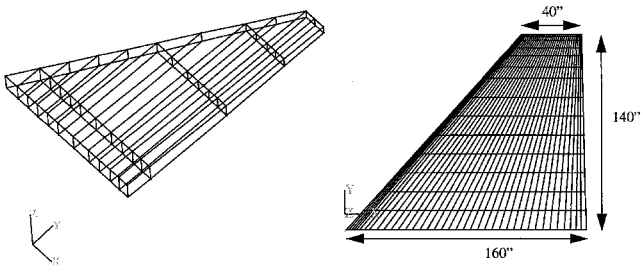

Fig. 5 Fighter wing finite element model, CFD mesh (39 × 15 on wing) and planform.

Description of Rectangular Wing Example

The rectangular wing selected was used in Ref. 15 to demonstrate transonic flutter predictions. The wing has a moderate aspect ratio, a 6% parabolic airfoil, and a uniform cantilever beam represents the structural model (Fig. 1). Rectangular wing structural parameters are as follows: mass = 11.19 slugs/ft, torsional moment of inertia = 29.145 slug-ft^2/ft, static unbalance = 6.705 slug-ft/ft^2, bending stiffness = 23.66E+6 lbs-ft^2, and torsional stiffness = 2.39E+6 lbs-ft^2. Calculated natural frequencies and modal descriptions are given in Table 1. The flight condition chosen is Mach number 0.85 and α_0 = 0.5 deg. The small disturbance model (Fig. 1) consists of a 60 × 23 × 40 mesh with 39 chordwise grids and 15 spanwise grids on the wing. Because the small disturbance mesh differed from the structural mesh, transformation of the mode shapes from the structural mesh to the CFD grid is required. This is accomplished by using the infinite plate spline in Ref. 16.

Static Aeroelastic and Flutter Analysis of Rectangular Wing

The analysis of the wing consists of static aeroelastic and flutter analyses. To perform a static aeroelastic analysis of the wing, a dynamic pressure has to be selected. Using the computational aeroelastic program–transonic small disturbance (CAP–TSD)[17] system to integrate the aeroelastic equations of motion in time, a flutter dynamic pressure ($q_f \approx 86.0$ psf) is found for $M_\infty = 0.85$ and $\alpha_0 = 0.5$ deg. This corresponds to a flutter frequency of $\omega_f \approx 2.09$ Hz and a flutter velocity of U_f = 948.9 ft/s. This flutter dynamic pressure is used for the static aeroelastic analysis and as a comparison to evaluate the accuracy of the flutter dynamic pressure calculated presently by the indicial response method (IRM) implemented into CAP–TSD.[9]

Using a dynamic pressure of 86.0 psf, a static aeroelastic equilibrium is determined. Figure 2 shows the static aeroelastic deformation of the wing. Figure 3 shows plots of coefficients of pressure for the upper surface (C_p^U), lower surface (C_p^L), and difference between the upper and lower surfaces (ΔC_p) of the wing at four spanwise stations for the given condition. These plots show that a shock has begun to develop on the upper surface of the wing that is stronger at the root and weakens as it progresses along the span. Using the static aeroelastic deformations as initial conditions, the indicial response method is used to determine the unsteady aerodynamic forces in the Laplace domain. Once in the Laplace domain, the unsteady aerodynamics are used in Eq. (1) for flutter analysis and Eq. (14) for the sensitivity analysis. Using Eq. (1) and a modified version of the automated structural optimization system (ASTROS),[1] q_f using the indicial aerodynamics is predicted to be 77.1 psf with a flutter frequency ω_f of 2.07 Hz and a flutter velocity U_f of 899.1 ft/s. This produces about a 5% difference in flutter velocity when compared to the flutter velocity found using time integration, which is considered acceptable. Figure 4 is a $U_\infty - g$ diagram of the flutter analysis. The computational resources necessary to determine the flutter parameters by the indicial response method (IRM) for this case requires approximately 20 min of YMP CPU. This includes both the static aeroelastic calculations and the indicial responses.

Sensitivity Analysis of the Rectangular Wing

Two design variables are selected for the wing: the height and width of the beam, which serve as the main and only spar for the wing. Assuming a rectangular cross section, the initial width (v_1) and height (v_2) of the section is found to be 0.2509 and 0.9092 ft, respectively. It is noted that these dimensions extend beyond the 6% parabolic airfoil used for the wing. This is because of the selection of a rectangular cross section of the main structural beam that serves no aerodynamic purpose.

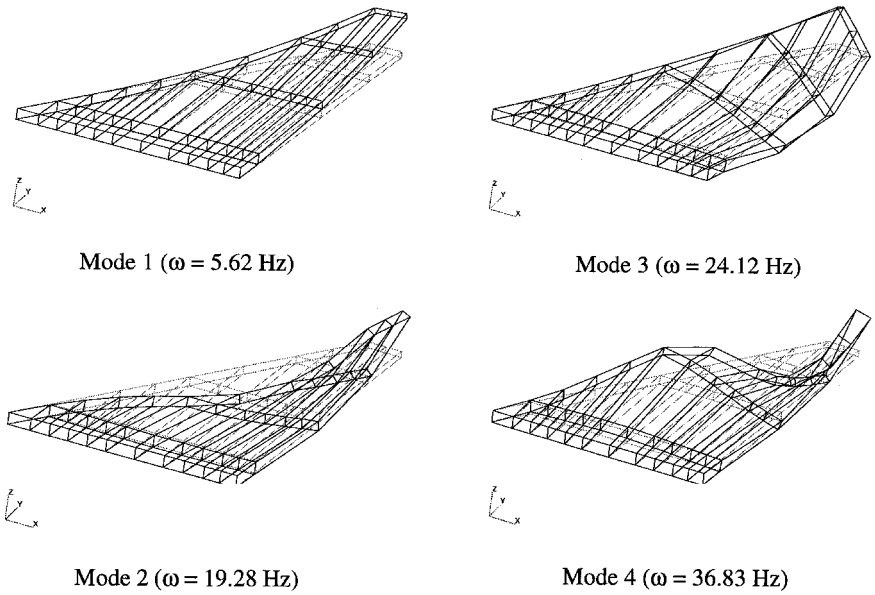

Fig. 6 Fighter wing first four fundamental mode shapes and frequencies.

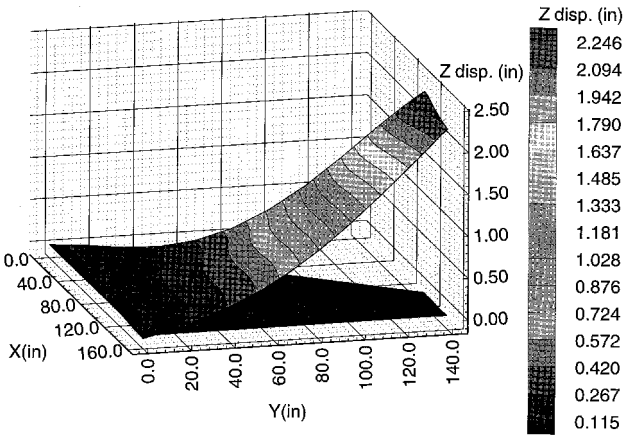

Fig. 7 Fighter wing static aeroelastic deformation (M_∞ = 0.93, α_0 = 0.5 deg, and q_∞ = 51.0 psi).

To demonstrate the sensitivity analysis calculation, a constraint is set to increase the flutter velocity by 15% (from 899.1 to 1122.8 ft/s). This translates to a constraint that requires the damping to be less than or equal to zero for velocities less than 1112.8 ft/s for all modes participating in the flutter analysis. The constraints are evaluated at four velocities for each mode and are found in Table 2. A positive value for a constraint indicates a violation, a negative value indicates satisfaction, and a value of zero is an indication that the constraint is exactly on the boundary between violation and satisfaction. The derivatives of the four constraints for mode 1 with respect to the design variables are calculated in five different fashions; two analytically and three by finite differences. Table 3 summarizes these results. The second column in Table 3 lists the sensitivities calculated using Eqs. (3), (5), and (14); these should compare to the finite difference sensitivities found in column three. Table 3 shows that for both v_1 and v_2 the analytic and finite difference are in excellent agreement (less than 1 and 5% for v_1 and v_2, respectively). Columns four and five of Table 3 are the sensitivities excluding the nonlinear term $(\partial[\bar{Q}(p)]/\partial\omega_l)(\partial\omega_l/\partial \boldsymbol{v}_s)$ in Eq. (14). Again, excellent agreement is found between the analytic and the finite difference sensitivities. When comparing columns two and four in Table 3, the effect of the nonlinear term $(\partial[\bar{Q}(p)]/\partial\omega_l)(\partial\omega_l/\partial v_s)$ can be evaluated. For v_1, the difference between columns two and four is, in general, less than 5%. For design variable v_2, comparing columns two and four indicates some differences between the sensitivities found including and excluding the nonlinear term when based on percentages. Care must be taken when evaluating these differences. The sensitivities of v_2 are one to two orders of magnitude smaller than the sensitivities associated with v_1 and are near zero. Although the percentage changes are significant when comparing the sensitivities for v_2 in columns two and four of Table 3, the absolute differences are negligible. This implies, at least for this problem, the $(\partial[Q(p)]/\partial\omega_l)(\partial\omega_l/\partial \boldsymbol{v}_s)$ term can be neglected resulting in a large computational savings (six CFD and about 1 h of Cray-YMP CPU).

As a final calculation, the sensitivities are determined by finite differences including the change of the $[\bar{M}]$, $[\bar{K}]$, and the aerodynamic matrix $[\bar{Q}(p)]$ with respect to the eigenmatrix $[\Phi]$ and the change of the eigenmatrix $[\Phi]$ with respect to $\boldsymbol{v}_i$. Neglecting these terms are some of the assumptions that lead to the derivation of Eq. (10). These sensitivities are found in column six of Table 3. These sensitivities agree well with those in columns two and three indicating that the assumptions made concerning the derivatives with respect to $[\Phi]$ are valid.

Description of Fighter Wing Example

This test case is a modified version of the sample case found in Ref. 18. For this work the wing structure is terminated at the wing root (no carry-through attachment) and the overall mass is scaled to obtain the desired natural frequencies. In addition, a 4% parabolic airfoil is employed over the entire wing to include thickness effects. Figure 5 shows the finite element model and the small-disturbance finite difference mesh that has 60 × 23 × 70 grids overall with 39 chordwise grids and 15 spanwise grids on wing. Here, only the first four natural vibration modes are used in the analyses. The mode shapes and the corresponding frequencies are presented in Fig. 6. The flight condition selected is Mach number 0.93 and an initial angle of attack of α_0 = 0.5 deg.

Static Aeroelastic and Flutter Analysis of Fighter Wing

As in the previous example, the analysis of the wing consists of static aeroelastic and flutter analyses. To perform a static aeroelastic analysis of the wing a dynamic pressure is required. Using the procedure outlined in the previous example, a flutter instability is determined with the following results: $q_f \approx$ 51.0 psi, $\omega_f \approx$ 19.5 Hz, and U_f = 12,459.0 in./s.

With a dynamic pressure of 51.0 psi, the static aeroelastic equilibrium is found for M = 0.93 and α_0 = 0.5 deg. Figure 7 shows the static deformation of the wing, whereas Fig. 8 shows plots of coefficients of pressure for the upper and lower sur-

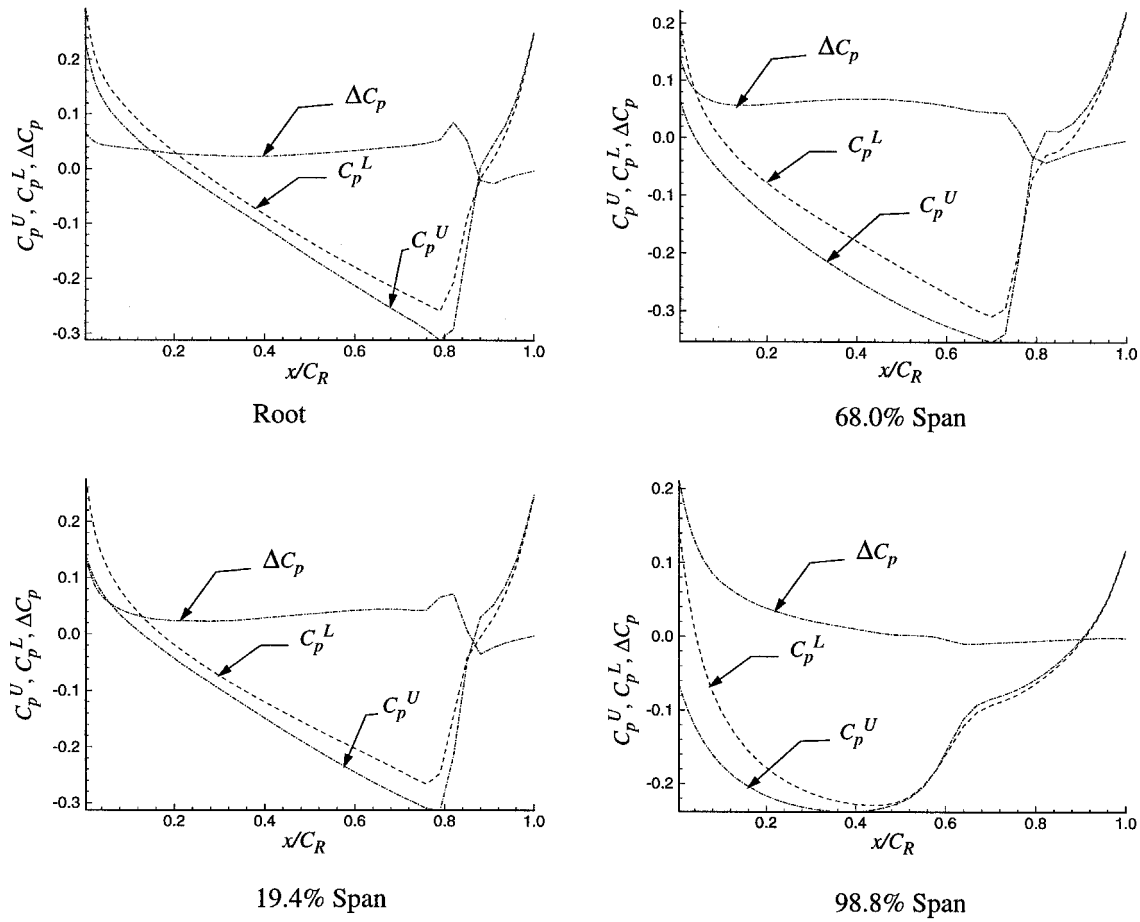

Fig. 8 Fighter wing pressure coefficients (M_∞ = 0.93, α_0 = 0.5 deg, and q_∞ = 51.0 psi).

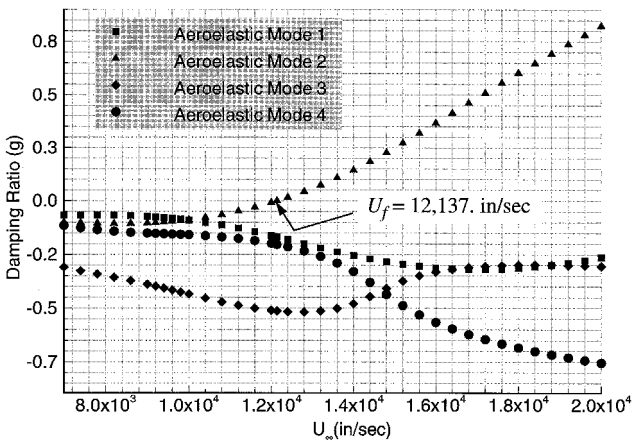

Fig. 9 Fighter wing U_∞ vs g (M_∞ = 0.93, α_0 = 0.5 deg, ρ_∞ = 6.571E−7 slinches/in.^{3}).

faces of the wing at four span stations. These plots show a fairly strong shock on the upper and lower surface at about 80% chord. Using the unsteady aerodynamics obtained by the IRM, a q_f is found to be 48.4 psi. The corresponding ω_f and U_f are 19.6 Hz and 12,137.0 in./s, respectively. These are in excellent agreement with the flutter results computed using time integration with CAP–TSD. Figure 9 is a U_∞–g diagram of the flutter analysis indicating that the second mode couples with the first mode to produce the instability for this case. The computational resources necessary to determine the flutter parameters by the IRM for this case is approximately 50 min of YMP CPU.

Table 4 Fighter wing constraint values[a]

Mode number	Constraint value @, in./s			
	11,000	12,000	13,500	15,000
1	−0.5966	−0.8035	−1.1640	−1.4500
2	−0.28215	−0.4002	0.4950	1.2485
3	−2.3970	−2.5530	−2.5250	−1.9500
4	−0.8538	−0.9871	−1.4050	−2.3170

[a]M_∞ = 0.93, α_0 = 0.5 deg, and ρ_∞ = 6.571E−7 slinches/in.^{3}.

Sensitivity Analysis of the Fighter Wing

The 26-structural design variable configuration of the wing found in Ref. 18 was selected for this study. To demonstrate the sensitivity analysis calculation, a constraint was set to increase the flutter velocity by 15%. The constraints were evaluated at four velocities for each mode and are found in Table 4. The derivative of the four constraints generated by mode 2 with respect to the design variable v_{16} associated with the top and bottom skins in bay two (bay 1 is next to wing root) are then calculated in five different fashions; two analytically and three by finite differences. Table 5 summarizes these results. As in the previous example, the analytic sensitivities in the second column should compare to the finite difference sensitivities found in column three. Comparison shows the largest difference of 7.5% occurring for the constraint at U_∞ = 12,000 in./s and the rest differing by less than 5%. These values are considered to be in good agreement. Columns four and five of Table 5 are once again the sensitivities excluding the nonlinear term $(\partial[\tilde{Q}(p)]/\partial\omega_l)(\partial\omega_l/\partial v_s)$ in Eq. (14). Again, the results agree between the analytic and the finite difference sensitivities (generally less than 8%). In Table 5, when comparing columns two to four, and three to five, the effect of the nonlinear term

Table 5 Fighter wing gradient terms[a]

$\frac{\partial Z_j}{\partial v_s}$	Includes $\frac{\partial[\bar{Q}]}{\partial v_s}$, no $\frac{\partial[\bar{Q}]}{\partial[\Phi]}$, $\frac{\partial[\Phi]}{\partial v_s}$		No $\frac{\partial[\bar{Q}]}{\partial v_s}$, no $\frac{\partial[\bar{Q}]}{\partial[\Phi]}$, $\frac{\partial[\Phi]}{\partial v_s}$		Includes $\frac{\partial[\bar{Q}]}{\partial v_s}$, includes $\frac{\partial[\bar{Q}]}{\partial[\Phi]}$, $\frac{\partial[\Phi]}{\partial v_s}$
	Analytical	Finite difference	Analytical	Finite difference	Finite difference
$\frac{\partial Z_{L_\infty}}{\partial v_{16}}$ = 11,000	−0.1742	−0.182	−0.1665	−0.1875	−0.1725
$\frac{\partial Z_{L_\infty}}{\partial v_{16}}$ = 12,000	−0.3170	−0.3424	−0.3191	−0.3390	−0.320
$\frac{\partial Z_{L_\infty}}{\partial v_{16}}$ = 13,500	−0.5675	−0.5895	−0.5654	−0.5960	−0.550
$\frac{\partial Z_{L_\infty}}{\partial v_{16}}$ = 15,000	−0.8418	−0.8600	−0.8380	−0.8600	−0.8150

[a] $M_\infty = 0.93$, $\alpha_0 = 0.5$ deg, and $\rho_\infty = 6.571\text{E}{-7}$ slinches/in.^{3}.

$(\partial[\bar{Q}(p)]/\partial\omega_l)(\partial\omega_l/\partial v_s)$ can be evaluated. In both cases the differences are less than 5%. Implying, as in the previous example, the nonlinear term can be neglected eliminating the need for 20 TSD time integrations (approximately 3 h of CPU on a Cray Y-MP for this example). This is a significant computational cost savings.

Finally, the sensitivities are determined by finite differences including the change with respect to the eigenmatrix $[\Phi]$. These sensitivities are found in column six of Table 5. These sensitivities agree well with those in columns two and three, reinforcing the validity of the assumptions made concerning the derivatives with respect to $[\Phi]$.

Concluding Remarks

The preceding is a method for calculating the sensitivities for transonic unsteady aeroelastic constraints with respect to structural design variables (skin thicknesses, spar thicknesses, spar cap cross-sectional areas, etc.). The method requires that the transonic unsteady aerodynamics be represented in the frequency or Laplace domain. In this work the IRM is used to transform time-domain aerodynamics into the Laplace domain. The time-domain unsteady aerodynamics are determined by solving the TSD equations. The indicial responses are performed about a static aeroelastic equilibrium found using the TSD equations for the steady aerodynamics. Once in the Laplace domain, the unsteady aerodynamics are used to develop semianalytic equations for the constraint sensitivities. These sensitivity equations include a nonlinear term that is calculated by finite differences at a considerable computational cost. This term arises because the indicial responses are performed about a static aeroelastic equilibrium. If a static rigid equilibrium is used instead, this term vanishes, producing fully analytic sensitivities. For the test cases chosen, it is found that this nonlinear term contributes little to the total gradient calculation and can be ignored. This eliminates $m(m + 1)$ (m being the number of modes participating in the design) CFD time integrations, a considerable computational savings. This translates into about 1 and 3 h of Cray Y-MP CPU savings for the rectangular wing and fighter wing, respectively. Further test cases need to be developed and examined to determine if the nonlinear term can be dismissed in general when using a static aeroelastic equilibrium as an initial condition for indicial responses. Finally, this method of sensitivity calculation enables formal unsteady aeroelastic optimization in the transonic flight regime.

References

[1] Neill, D. J., Johnson, E. H., and Herendeen, D. L., "Automated Structural Optimization System (ASTROS), Volume II-User's Manual," Air Force Wright Aeronautical Labs., TR-883028, Vol. 2, April 1988.

[2] Johnson, E. H., and Reymond, M. A., "Multidisciplinary Aeroelastic Analysis and Design Using MSC/NASTRAN," AIAA Paper 91-1097, April 1991.

[3] Kapania, R. K., "Sensitivity Analysis of Dynamic Aeroelastic Responses," AGARD Rept. 784, Feb. 1992, pp. 3-1–3-12.

[4] Kapania, R. K., Issac, J. C., Barthelemy, J. F. M., "Sensitivity Analysis of Flutter Response of a Typical Section and a Wing in Transonic Flow," AIAA Paper 93-1646, April 1993.

[5] Leishman, J. G., and Nguyen, K. Q., "State-Space Representation of Unsteady Airfoil Behavior," *AIAA Journal*, Vol. 28, No. 5, 1990, pp. 836–844.

[6] Korivi, V. M., Taylor, A. C., Newman, P. A., Hou, G. J-W., and Jones, H. E., "An Approximately Factored Incremental Strategy for Calculating Consistent Discrete Aerodynamic Sensitivity Derivatives," AIAA Paper 92-4746, Sept. 1992.

[7] Borggaard, J., and Burns, J., "A Sensitivity Equation Approach to Shape Optimization in Fluid Flows," NASA CR 191598, Jan. 1994.

[8] Stephenson, A. M., "Linearized Transonic Aerodynamics for Aircraft Design," M.S. Thesis, Univ. of Dayton, Dayton, OH, July 1992.

[9] Kolonay, R. M., "Transonic Unsteady Aeroelastic Analysis for the Multidisciplinary Design Environment," AIAA Paper 95-1285, April 1995.

[10] Johnson, E. H., and Venkayya, V. B., "Automated Structural Optimization System (ASTROS), Volume 1-Theoretical Manual," U.S. Air Force Wright Aeronautical Labs., TR-88,3028, Vol. 1, Dec. 1988.

[11] Hajela, P., "A Root Locus Based Flutter Synthesis Procedure," AIAA Paper 83-0063, Jan. 1983.

[12] Rudisill, S. C., and Bhatia, G. K., "Optimization of Complex Structures to Satisfy Flutter Requirements," *AIAA Journal*, Vol. 9, No. 8, 1971, pp. 1487–1491.

[13] Haftka, R. T., Jr. and Yates, C. E., "Repetitive Flutter Calculations in Structural Design," *Journal of Aircraft*, Vol. 13, No. 7, 1976, pp. 454–461.

[14] Canfield, R. A., and Jacques, D., "Effect of Modal Sensitivity on Flutter Eigenvalue Derivatives," AIAA Paper 94-1545, April 1994.

[15] Borland, C. J., "XTRAN3S-Transonic Steady and Unsteady Aerodynamics for Aeroelastic Applications," U.S. Air Force Wright Aeronautical Labs., TR-85-3124, Vol. 1, Jan. 1986.

[16] Harder, R. L., and Desmarais, R. N., "Interpolation Using Surface Splines," *Journal of Aircraft*, Vol. 9, No. 2, 1972, pp. 189–191.

[17] Batina, J. T., "A Finite-Difference Approximate-Factorization Algorithm for Solution of the Unsteady Transonic Small-Disturbance Equation," NASA TP 3129, Jan. 1992.

[18] Striz, A. G., and Venkayya, V. B., "Influence of Structural and Aerodynamic Modeling on Optimization with Flutter Constraint," *Proceedings of the 3rd USAF/NASA Symposium on Recent Advances in Multidisciplinary Analysis and Optimization* (San Francisco, CA), Anamet Labs., Inc., Haywood, CA, 1990, pp. 431–438.